Body Feature Intercomparison of Specific Absorption Rate Induced by High-Power, Portable, and Broadband Electromagnetic Sources

Eliana Canicatti, Danilo Brizi, Angelica Masi, Nunzia Fontana, and Agostino Monorchio

This work presents an electromagnetic exposure intercomparison among representative human models with different body features (i.e., height, weight, and age) and genders when exposed to near-field, high-power, and broadband devices. Such devices are commonly used in the military field for communication and jamming purposes. With the aim of obtaining accurate and detailed whole-body-averaged (WBA) specific absorption rate (SAR) and 10-g SAR evaluations, a realistic scenario is numerically simulated. Three different antenna configurations are adopted, faithfully reproducing the radiative characteristics and operative frequency bands of similar devices (40–2,700 MHz). Then, we equally expose in the working band three different human body models (Hugo, Duke, and Ella). The obtained results show that the WBA-SAR is mainly related to the total body weight, as expected from its definition. Conversely, the 10-g SAR varies along with the frequency range, and different results are observed for each human model. Guidelines for exposure reduction and physical considerations are also presented. This study can be a useful reference for conducting complete and accurate radio-frequency (RF) dosimetry analysis for such particular and high-risk devices, differentiating the study for different genders and body shapes of human body models.

Digital Object Identifier 10.1109/MAP.2023.3280840
Date of current version: 8 August 2023

EDITOR'S NOTE

Asimina Kiourti

This article for the "Bioelectromagnetics" column provides a comparative dosimetry study for high-power broadband devices with wireless functionality. The study considers three different antenna configurations in the 40- to 2,700-MHz frequency range as well as three different anatomical human body models (male and female), with a focus in the near-field region. The results provide informative insights on the formation and location of hot spots with respect to intersubject variability.

This column welcomes articles on biomedical applications of electromagnetics, antennas, and propagation in terms of research, education, outreach, and more. If you are interested in contributing, please e-mail me at kiourti.1@osu.edu.

INTRODUCTION

The problem of the exponentially rising exposure of the general population to electromagnetic fields (EMFs) has raised the attention of the scientific community regarding the possible risks for human health [1]. Accordingly, the evaluation of the electromagnetic energy deposition on biological tissues is fundamental to assess whether a radiative source can be safely used near or in contact with the human body. As a metric, the SAR (watts per kilogram) has been defined, and it is generally adopted. Hence, to protect the population from massive exposure to EMFs, the International Commission on Non-Ionizing Radiation Protection (ICNIRP) and IEEE have developed safety guidelines [2] and standards [3], respectively. These guidelines provide both methods for measuring the SAR and limit thresholds to effectively assess when a device becomes potentially hazardous for human health.

Experimental evidence has shown that a SAR value greater than 4 W/kg, averaged over the total body volume (i.e., the WBA-SAR), can lead to irreversible biological effects; this is due to the fact that such energy deposition can

easily produce an overall body temperature increase of about 1 °C when the exposure exceeds 30 min [4], [5]. Therefore, this value has been adopted in the international standards as a reference safety margin. In particular, the whole-body exposure (WBA-SAR) limits have been cautiously set at 0.4 W/kg (10 times lower than the aforementioned threshold value) for workers and 0.08 W/kg (50 times lower than the aforementioned threshold value) for the general public [2], [3], respectively. In addition to the whole-body exposure, another fundamental aspect is the localized near-field exposure assessment by means of the local SAR distribution. Since the use of radiating devices closely placed or direct in contact to the human body is dramatically increasing, an accurate estimation of localized heating is needed. To this end, limits on the averaged peak SAR value on 10 g of tissue in international standards have also been introduced. These local SAR limits have been obtained by increasing the basic WBA margin by a factor of 25. Hence, the local SAR limit was set at 10 W/kg for workers and 2 W/kg for the public [2], [3].

In the light of the preceding considerations, it is evident that a correct SAR level estimation is required for a careful safety assessment of a radiating device. Currently, some works in the literature have explored the exposure level quantification for mobile devices, tablets, and smartwatches [6], [7], [8], [9], [10], [11]; moreover, the SAR rating for wearable systems have been investigated, such as for devices monitoring biological parameters or prosthetic implants [12], [13], [14], [15], [16]. Generally, the common feature of all these devices is their operative modality; they work in the near-field region but in a very narrow frequency band or even a single frequency, as in the case of biomedical monitoring systems.

Nevertheless, there are commercially available high-power portable electromagnetic devices that act both in the near-field region and in a wider frequency band. These types of devices are usually employed for military applications in the form of wearable backpack systems for communications, jamming, or situational awareness [17].

In [18], the effect of the aforementioned radiative sources on a specific human body voxel model has been evaluated, and guidelines for the reduction of exposure levels have been defined. However, it is acknowledged that the human population has strongly variable anatomical characteristics in terms of height and weight; furthermore, it is well known that body composition differs among males and females, especially in terms of adipose content [19] and as a function of age. As a consequence, different bodies can be subjected to different levels of exposure in the presence of the same radiative source [20], [21]. Several works in the literature have carried out the SAR evaluation for different body models and genders in the far-field region by using a vertically polarized impinging plane wave [22], [23], [24], [25]. Nonetheless, the use of similar radiative sources does not provide a realistic SAR assessment since plane waves never occur in reality, and often, the human body is illuminated within the near-field region.

To overcome these limitations, we performed a broadband SAR analysis in the near-field region, using realistic high-power (60-W) radiating sources operating on a wider frequency band (40–2,700 MHz). Three different standard voxel phantom models (Hugo [26], Duke, and Ella [27]) have been adopted; they represent two men of different ages and body conformations and a woman. By considering the dispersive dielectric properties of the tissues in the entire frequency band, the exposure levels and localization of SAR hot spots were accurately assessed. In [28], some preliminary results related to the WBA-SAR have already been presented. Since these results have shown a significantly higher SAR level for the female model, we have carried out a more in-depth and accurate analysis. Important information can be inferred from this study by determining how hot spot locations vary with gender and body conformation. To the best of our knowledge, such an analysis has not yet been performed in the literature. The present work is organized as follows. The "Problem Statement" section presents the problem statement and purpose of the study. The "Method" section deals with the description of human body voxel models that have been adopted and the settings of the numerical scenario. In the "Numerical Results" section, numerical results are presented and discussed. Finally, conclusions are described.

PROBLEM STATEMENT

The aim of this study is the intercomparison of the electromagnetic energy absorption among human models, differing in gender and body features (i.e., height, weight, and age), when they are exposed to portable, high-range, and broadband electromagnetic devices. As mentioned, similar systems are extremely common in military applications, where they are used in tactical communication or situational awareness. In the context of the ICNIRP and IEEE international norms [2], [3], the EMF exposure of workers represents a significant health risk; hence, it is necessary to assess whether such equipment can be safely used [29] without causing adverse biological effects.

To evaluate this problem in an accurate way, a realistic near-field scenario has been set up. We have considered three standard voxel human models (Hugo, Duke, and Ella; Figure 1) representing adult people of a different sex, age, and body conformation. Each model was equipped with a portable backpack system that simulates a typical device used in military communication. A similar methodology has already been developed in [18] for a single human body model; herein, it has been extended to the young male (Duke) and female (Ella) models.

As depicted in Figure 2, the system is characterized by a backpack closely placed to the body. To simulate a realistic communication or jamming application, the device operates on a wide bandwidth (40–2,700 MHz); in fact, these systems are equipped with an arrangement of several monopole and dipole antennas switched on according to the transmission radio communication band. In addition, since this type of system transmits high-intensity signals, its input power has been set at 60 W.

To summarize, this study is aimed at providing a general safety assessment of

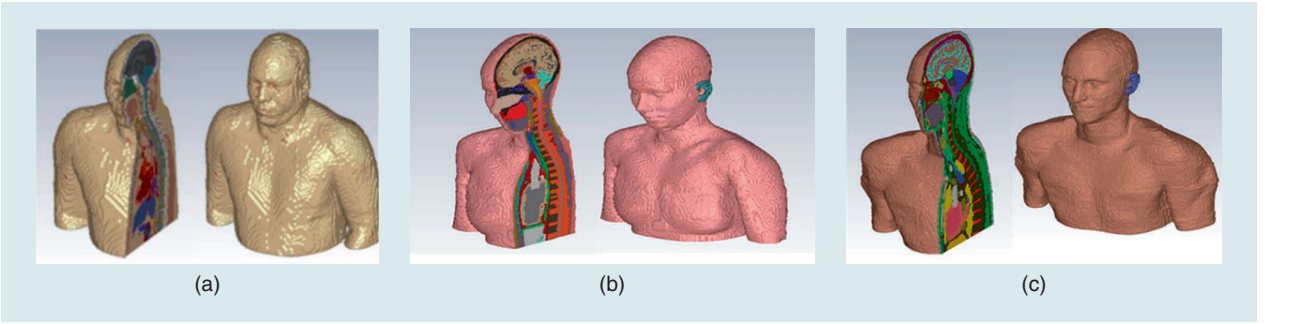

FIGURE 1. The sectional and half-bust voxel-based human models: (a) Hugo, (b) Ella, and (c) Duke.

high-power broadband devices for different categories of users, exploring how different genders and ages may affect the SAR deposition.

METHOD

VOXEL ANATOMICAL BODY MODEL

The SAR evaluation and related dosimetry studies cannot be experimentally conducted on actual human bodies since this assessment is practically unfeasible. Besides, realizing biological phantoms able to actually replicate the inhomogeneities of human tissues is still a challenge. Therefore, to overcome these limitations, extremely accurate anthropomorphic numerical phantoms have been developed, starting from tomography data, to be used in SAR assessment.

As stated, three human body models representative of gender and body conformation diversity have been employed to obtain results as accurate as possible in terms of the exposure level quantification of portable device antennas. As shown in Figure 1, such voxel models are Hugo, Duke, and Ella, respectively [28].

As described in [18], Hugo is probably the most popular and adopted voxel model [26]. It is characterized by high-fidelity anatomical detail acquired on a real human body by using high-resolution magnetic resonance imaging (MRI) data. This activity was carried out as part of the Visible Human Project [31] developed by the U.S. National Institute of Health. This phantom represents a 38-year-old man; his digitalized body model presents 32 different tissues with a voxel resolution that can range from approximately $8 \times 8 \times 8$ mm^3 to $1 \times 1 \times 1$ mm^3.

The other two models, Duke and Ella, represent a 34-year-old man and a 26-year-old woman, respectively. They are part of the Virtual Family, a project carried out in collaboration with the U.S. Food and Drug Administration, the Foundation for Research on Information Technologies in Society, and other academic and industrial partners [32]. Also, in this case, the numerical models have been obtained by referring to high-resolution MRI data acquired on healthy volunteers; their inner organs and tissues are featured by highly detailed 3D CAD objects with a voxel resolution ranging from $5 \times 5 \times 5$ mm^3 to $0.5 \times 0.5 \times 0.5$ mm^3. Their features are listed in Table 1.

As already highlighted for the Hugo model [18], these standard phantoms exhibit tissue dielectric properties evaluated only for a discrete number of frequencies. To perform an accurate broadband SAR assessment, the dielectric properties dataset has been customized. In more detail, by implementing the most widely used dispersive model in the literature, that is, the Gabriel and Gabriel model [33], we have calculated the dielectric parameters in the entire frequency range for each tissue. Consequently, the voxel model became broadband, allowing much greater SAR estimation accuracy.

To further optimize the numerical setup, it is necessary to evaluate the optimal voxel resolution for full-wave

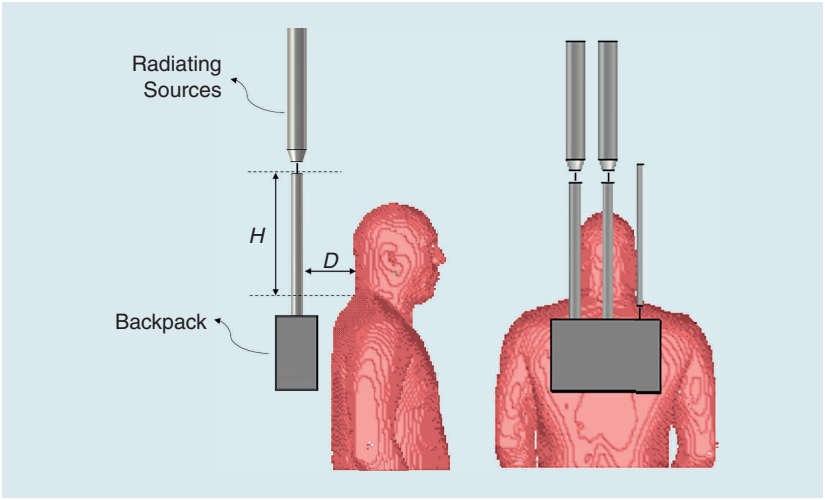

FIGURE 2. Typical portable military equipment.

TABLE 1. THE CHARACTERISTICS OF THE THREE ANATOMICAL HUMAN BODY MODELS.

Characteristic	Hugo	Ella	Duke
Sex	Male	Female	Male
Number of tissues	32	74	77
Body conformation	Fat	Slim	Slim
Height (m)	1.87	1.6	1.74
Weight (kg)	113	58	70

simulations. Although a finer voxel resolution naturally brings more accurate results, computational resources and simulation time can be prohibitive. Thus, in [18], a final voxel resolution of 4 × 4 × 4 mm has been chosen for the Hugo model as a good compromise between the accuracy of the SAR calculation and the simulation computational burden. This choice has been suggested by [34] and [35], in which the authors stated that the variation of the voxel size had a negligible effect on the SAR estimation and that the use of a finer resolution is necessary only to calculate small body structures and organs (e.g., eyes and the thyroid).

Finally, we have also implemented this choice for the Duke and Ella models by adopting a voxel resolution of 5 × 5 × 5 mm [28], based on the previous considerations and in accordance with [36].

RADIATING SOURCE MODEL

In a typical arrangement, military backpack devices include a set of antennas, mainly monopoles and dipoles, operating on different frequency ranges to cover the entire radio communications band. In [18], three different antennas have been specifically designed to faithfully represent the behavior of such radiative systems.

The first type is a quarter-wavelength monopole working in the 40–530-MHz band. It consists of an upright cylindrical-shaped conductor mounted perpendicularly on a perfectly conductive metal box used as a ground plane [Figure 3(a)]. The monopole has been tuned and matched to be operative in the entire 40–530-MHz band by gradually changing its electrical length.

The second type [Figure 3(b)] consists of an ultrawideband (UWB) dipole. In particular, two cylindrical rods with tapered ends are employed to obtain broadband impedance matching. From this general conception, two antennas have been designed by simply rescaling their dimensions: the dipoles were appropriately designed to accomplish frequency tuning and adequate impedance matching by maintaining their electrical length in the desired frequency band by exhibiting a minimum –10-dB matching level in both free space and in the presence of a biological load. Thus, we reproduced, with high precision, the typical performance of backpack devices, which often include electronic circuitry that matches the antenna impedance to work correctly with different operators. Hence, we ensured that the various antenna designs were functioning correctly and that over 90% of the amplifier's input power was supplied to the radiating system. Therefore, the two designed UWB dipoles work in the band between 530 and 1,800 MHz and 1,800–2,700 MHz, respectively.

We carried out the antenna design by using CST Studio Suite (Dassault Systems, France) electromagnetic software.

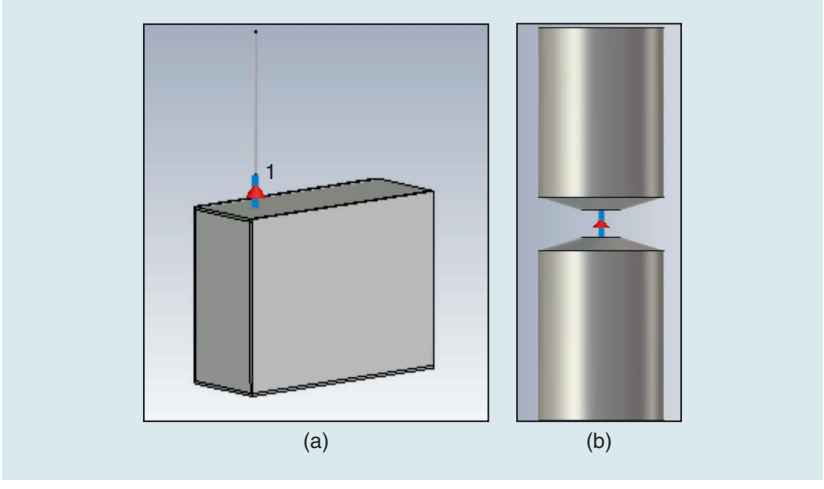

FIGURE 3. The radiating broadband device. (a) A quarter-wavelength monopole operating in the 40–530-MHz frequency range. (b) The general configuration of the ultrawideband dipole antenna.

In [18], we have shown the antennas' performance and radiative characteristics both in free space and in the presence of the numerical model Hugo. Herein, we have simulated the antennas in the presence of the other two voxel-based models, showing almost unaltered radiation patterns and good matching in terms of the reflection coefficient, under the threshold of –10 dB (Figure 4).

As illustrated in Figure 4, the degree of electromagnetic coupling varies according to the scenario. This phenomenon occurs because a biological load affects the antennas' input impedance. If an antenna is designed to transmit in free space, the unavoidable mismatch induced by loading will result in a decrease in transmitted power and, consequently, an increase in the reflection coefficient. Part of the reflected energy couples to the generator load through the antenna port, altering the input impedance and antenna matching. Hence, based on the latter considerations, it is also possible to conclude that, since the three voxel-based human models differ in height and body features, the incident wave that is partially absorbed and partially reflected also differs, determining a different reflection coefficient.

COMPLETE NEAR-FIELD NUMERICAL SCENARIO

To perform the full-wave simulations, a time-domain numerical electromagnetic algorithm has been employed, namely, the Finite Integration Technique (FIT). This choice was motivated by the memory-efficient capability and flexibility with respect to different materials and complex geometries of the FIT technique. The WBA-SAR value in the solver is obtained by dividing the total power absorbed in the human body by the full body weight. Conversely, local SAR values are averaged in a tissue mass of 10 g, as specified in the international ICNIRP norms [37].

To simulate real exposure conditions and the use of such backpack devices in military fields, we have chosen three different exposure scenarios for the three voxel-based human models. As in [18] and [28], the position of the radiative sources with respect to the human

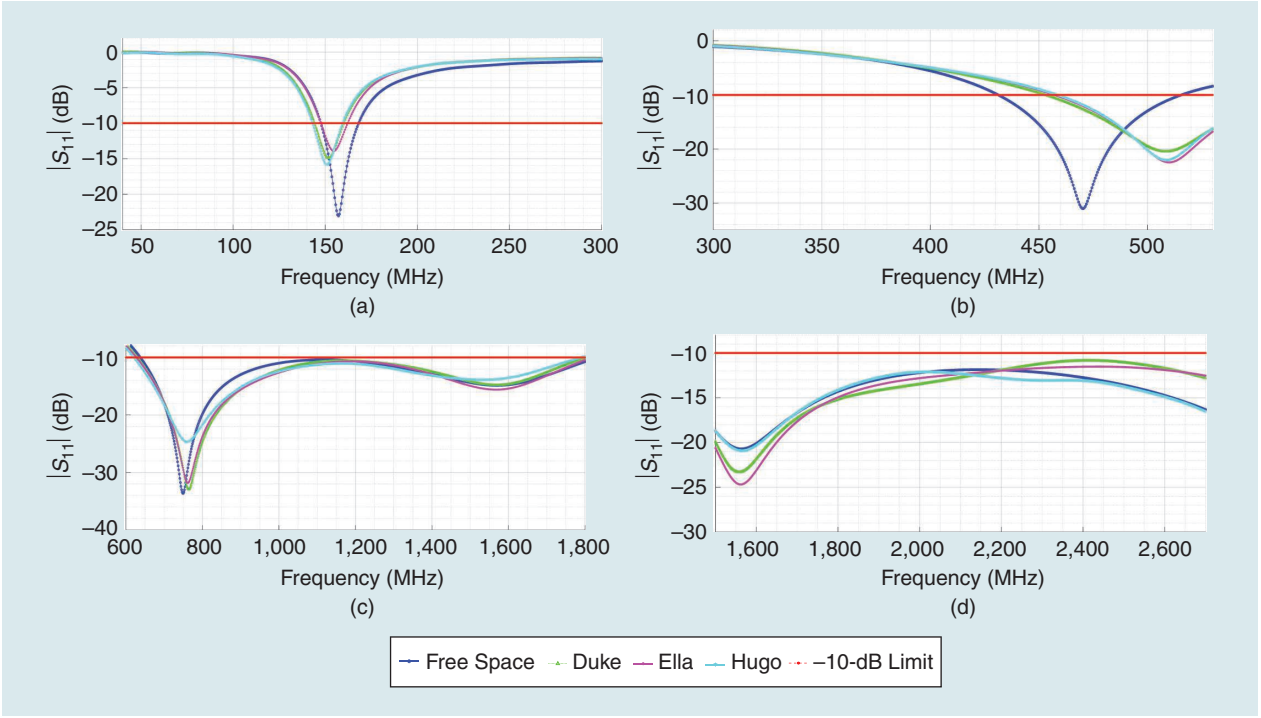

FIGURE 4. The S_{11} parameter of the previously described antennas in free space and the presence of the voxel-based human bodies (Hugo, Duke, and Ella): the (a) S_{11} of the monopole tuned at 150 MHz, (b) S_{11} of the monopole tuned at 500 MHz, and (c) S_{11} of the UWB dipole antenna operating in the range of 600–1,800 MHz and (d) 1,800–2,700 MHz.

models has been fixed at 13 cm from the neck and 3 cm from the shoulders.

In the first configuration, each voxel phantom is illuminated by the tuned monopole antenna, operating in the frequency band of 40–530 MHz, as depicted in Figure 5(a)–(c). Each model is chosen and assumed to be standing in free space and considered barefoot. Although in [23] and [38] it is reported that the maximum SAR is achieved when the incident electric field is vertically polarized and the model is barefoot on a ground plane, simulations with the radiative source placed in the near field were carried out in [18], observing that no significant variation in the results comes from the ground plane presence or absence.

On the other hand, in the second and third configurations, the three voxel-based models are in the presence of the UWB dipole antennas, operating in their proper frequency band. In this case, according to the considerations reported in [18], we have adopted the three models in the form of a half bust [Figure 6(a)–(c)] since the higher operative frequencies minimally influence the SAR deposition in the lower part of the body.

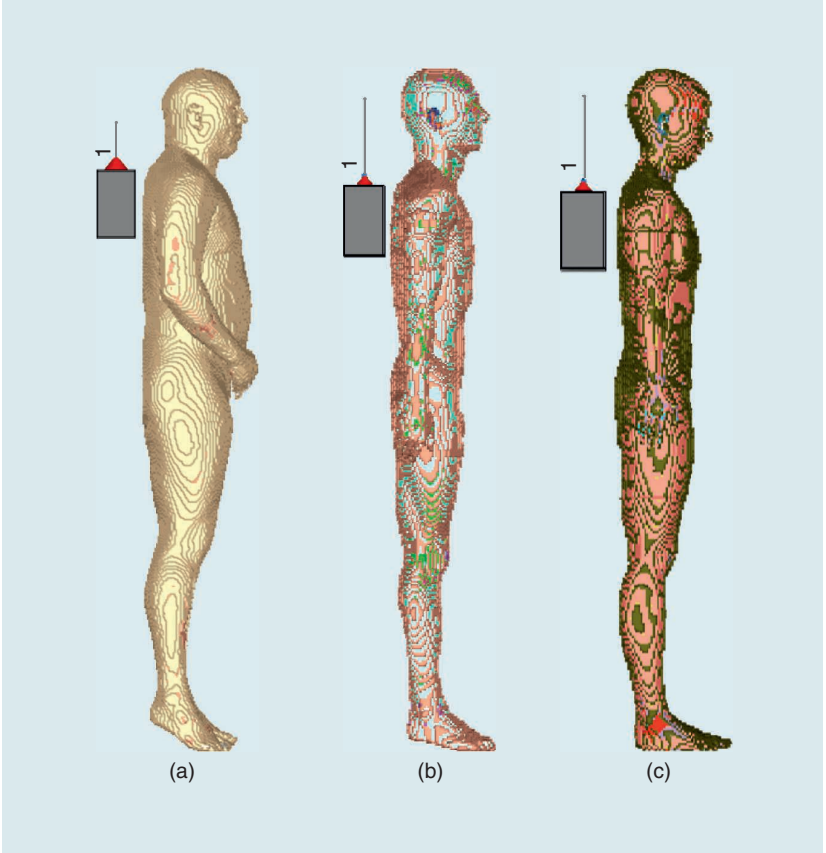

FIGURE 5. The first exposure configuration: the tuned monopole antenna operating in frequency range of 40–530 MHz. The (a) Hugo full-body model, (b) Duke full-body model, and (c) Ella full-body model.

All simulations were performed in the continuous wave condition since this is the worst exposure condition, as derived from the results of the multiphysics analysis carried out in [18] and [37].

NUMERICAL RESULTS

In this section, we present the WBA-SAR and 10-g SAR numerical results related to the three scenarios presented in Figures 5 and 6, respectively. Such results refer to a peak input power equal to 1 W. Notably, by setting the peak input power to 1 W, we aimed to make our study generalizable and a useful resource for doing comprehensive and precise RF dosimetry analyses on similar devices with different peak input power. Since such backpack military devices usually work at input powers levels equal to 60 W and an assumed system linearity characteristic, we implemented the following scaling formula [18] in the postprocessing procedure:

$$\mathrm{SAR}_{10g,\mathrm{new}} = \mathrm{SAR}_{10g,1W}\frac{P_{\mathrm{new}}}{P_{1W}}. \quad (1)$$

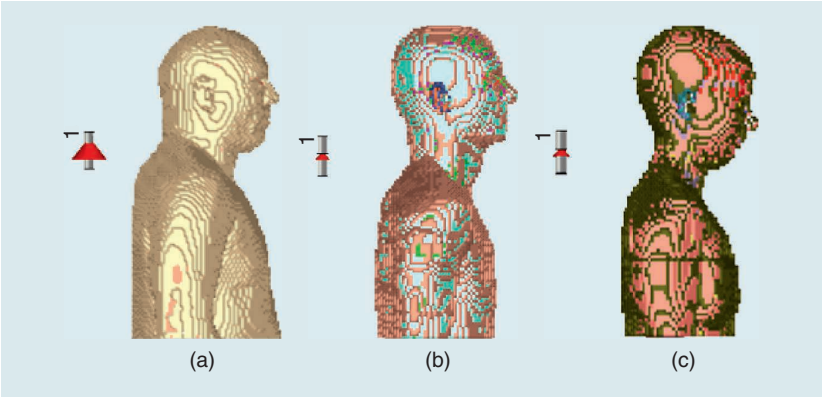

FIGURE 6. The second and third exposure configurations: the UWB dipole antenna operating in frequency ranges of 600–1,800 MHz and 1,500–2,700 MHz. The (a) Hugo half-bust model, (b) Duke half-bust model, and (c) Ella half-bust model.

WBA-SAR AND 10-G SAR ANALYSIS

The simulations have been executed by adopting a frequency sampling equal to

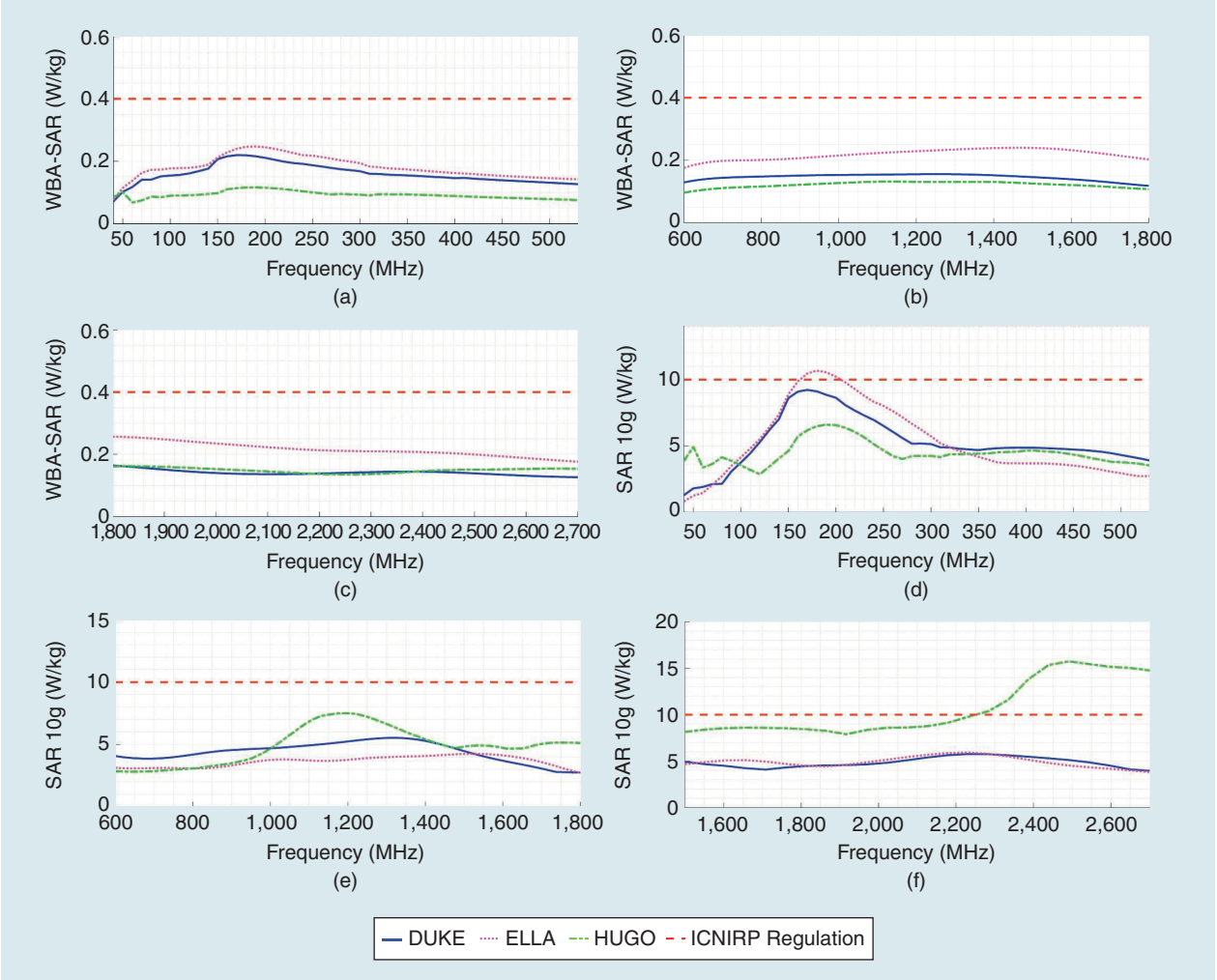

FIGURE 7. The WBA-SAR trend for a peak input power equal to 60 W: (a) 40–530 MHz, (b) 600–1,800 MHz, and (c) 1,500–2,700 MHz. The 10-g SAR trend for a peak input power equal to 60 W: (d) 40–530 MHz, (e) 600–1,800 MHz, and (f) 1,500–2,700 MHz.

10 MHz in the frequency range up to 1,800 MHz, whereas a coarser sampling of 50 MHz in the frequency range of 1,500–2,700 MHz has been chosen. The last choice is related to the SAR dependence with respect to the dispersive tissue characteristics, whose trend becomes stable at higher frequencies [33].

Then, we processed the collected data through an in-house postprocessing algorithm. Figure 7(a)–(c) represents the WBA-SAR results on the three subbands for each numerical voxel model. In agreement with [39], the results have general behavior that is similar in each case despite the substantial differences among the phantom models.

The last obtained result proves that electromagnetic energy absorption does not depend on body shape but on the considered radiative source. Nonetheless, it must be noticed that the WBA-SAR values' amplitude is greater in the female model than in the male ones; however, the last result is due to the WBA-SAR definition itself: the total power absorbed by the whole body over the total body weight, which is lower in the female model [40].

Generally, the WBA-SAR is a parameter used to evaluate the effect of far-field sources (i.e., plane waves and radar [41]); since such radiative sources are localized and placed close to the human body, the local 10-g SAR evaluation is more appropriate for near-field applications (e.g., as usually adopted for mobile terminals too).

By adopting the same postprocessing algorithm, the results in terms of the 10-g SAR have been provided in Figure 7(d)–(f). In the first subband, the results are in good agreement among the models. In fact, there is a 10-g SAR peak for each voxel model at a frequency around 170 MHz. The reason is to be ascribed to the antenna length (1.7 m), which is comparable to the heights of the voxel numerical models at this frequency. Thus, a resonance phenomenon that amplifies the fields and absorbed power is present [36]. However, a substantial difference in absorption between the female model and the male counterparts can be appreciated.

These results are in line with those described in [23] and [25] since the fat tissue percentage in women (i.e., subcutaneous adipose tissue and breast mammary tissue [42]) is higher than in men. Due to its dielectric properties, fat is a good propagation medium inside the human body at lower frequencies [43], [44]. So, the exposure levels may exceed the limits imposed by [2] for female

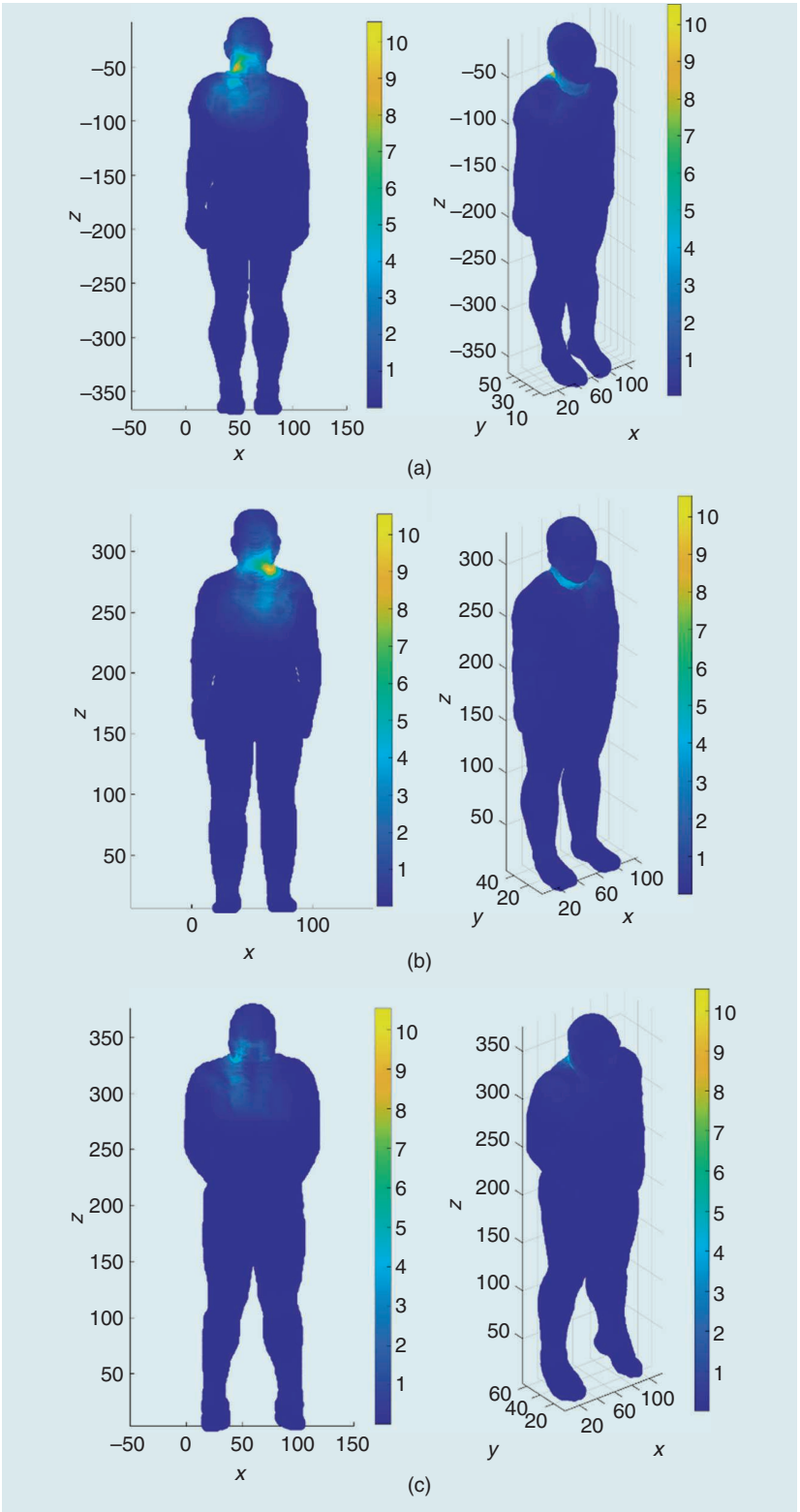

FIGURE 8. The maximum 10-g SAR hot spot localization for a peak input power equal to 60 W in the frequency range of 40–530 MHz: (a) Duke, (b) Ella, and (c) Hugo.

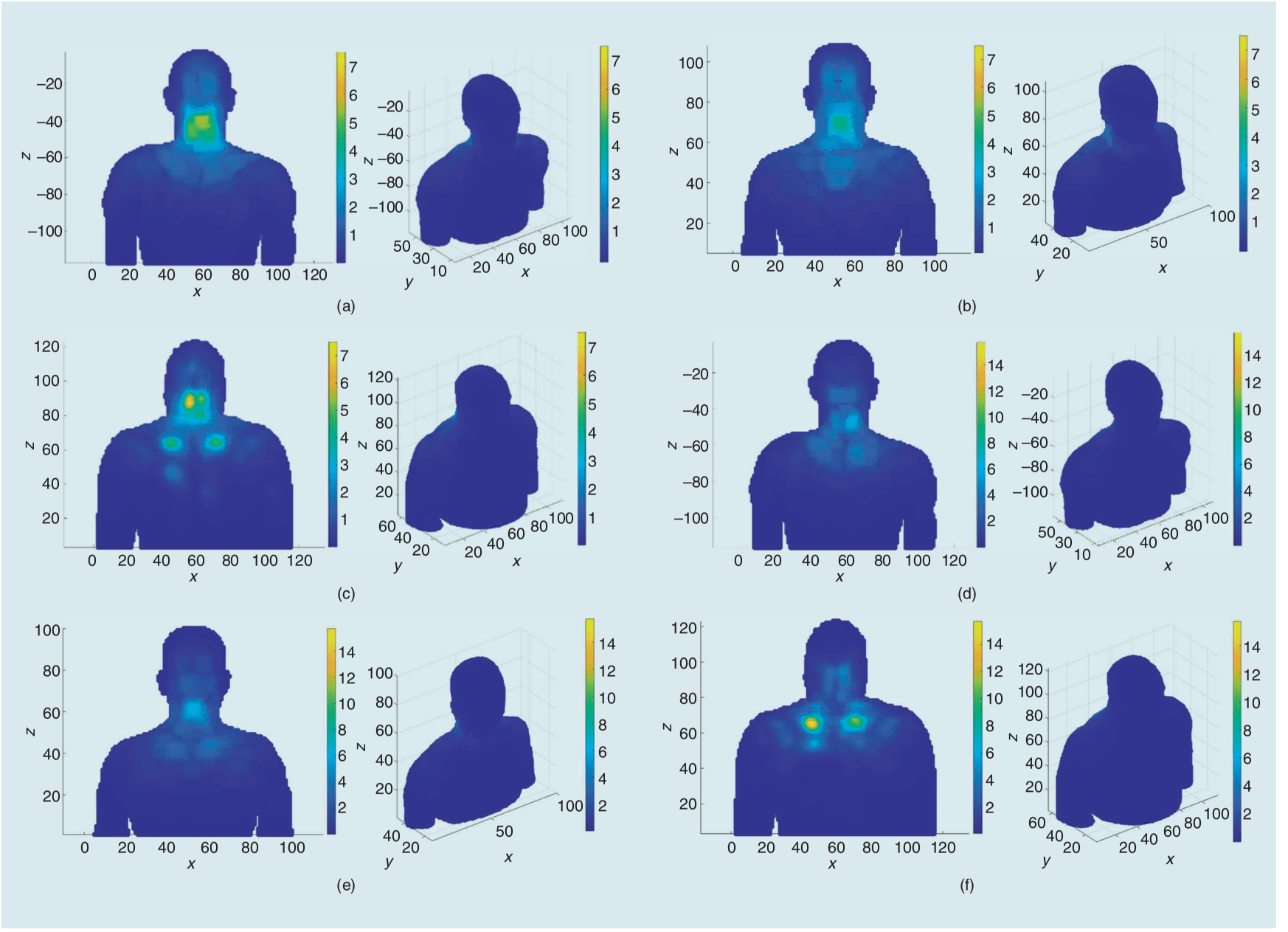

FIGURE 9. The maximum 10-g SAR hot spot localization for a peak input power equal to 60 W in the frequency range of 600–1,800 MHz: (a) Duke, (b) Ella, and (c) Hugo. The maximum 10-g SAR hot spot localization for a peak input power equal to 60 W in the frequency range of 1,500–2,700 MHz: (d) Duke, (e) Ella, and (f) Hugo.

models; therefore, guidelines for SAR exposure reduction must be adopted, as reported in [18].

Regarding the subbands in 600–1,800 MHz and 1,500–2,700 MHz, lower 10-g SAR values are found in the Duke and Ella models, compared to the Hugo one. However, these are due to the intrinsic conformation of the Hugo model, which has an outer layer mainly consisting of fat, without the skin layer (differing from Duke and Ella). It is possible to conclude that the presence of skin increases the reflection at higher frequencies and generally reduces SAR levels below the norm limitations [25].

To conclude the exposure risk assessment, we evaluated the localization and identification of the hot spots within the three voxel human body models. Specifically, we have elaborated the 2D and 3D SAR maps for each sampled frequency and visualized them for different geometric planes.

In this study, we report the SAR maps for each voxel model, corresponding to the maximum 10-g SAR peaks identified on each respective subband. To understand the position of the hot spots within the body, we have depicted the maps both in the coronal plane and a 3D view (Figures 8 and 9). Furthermore, in Figure 10, the maximum values and positions of the hot spots for each model on each respective subband are summarized.

The hot spot distributions were scaled to the maximum SAR 10-g value among the three models to highlight qualitative and quantitative variation between SAR distributions for the three human voxel models. From the 2D maps, it is possible to observe how hot spots change their position according to the frequency band. In addition, it is interesting to note how exposure levels vary from model to model. In general, it can be inferred that hot spots tend to cluster near the shoulders and neck, i.e., near radiative sources, as expected.

ASSESSMENT OF THE SKIN EFFECT ON THE VOXEL-BASED MODELS

When the human body is excited by the antennas, part of the signal is scattered away, and part is absorbed. The reflection level mainly depends on the air–tissue interface, which can determine higher exposure levels and, consequently, higher SAR values. In particular, this phenomenon has been observed at higher frequencies (1,500–2,700 MHz) since the SAR trend [Figure 7(f)] is in good agreement between the Duke and Ella models but significantly higher in Hugo.

Therefore, we have carried out further investigations; by analyzing the three voxel models in detail, we have observed that Duke and Ella have skin outer layers, while a skin outer layer is not present in the Hugo numerical model.

Therefore, it was inferred that the presence of skin can affect the EMF reflection and, consequently, the electromagnetic energy absorption in the human body. In [45] and [46], the absorption and reflection levels of a plane wave referred to a layered model with and without skin were evaluated. The authors found that the reflection coefficients among the two models are different, and this phenomenon is explained by the presence of skin. Furthermore, when the skin layer is removed, the reflection coefficient is close to the model without it.

Based on these considerations, we simulated two stratified cylinders [Figure 11(a) and (b)] equal to Hugo's torso size (60 cm in height, 38 cm in diameter), consisting of an inner muscle layer and an intermediate 7-mm fat layer [47]. Only one cylinder has the outer 2-mm skin layer [30], [48] [Figure 11(b)]. The

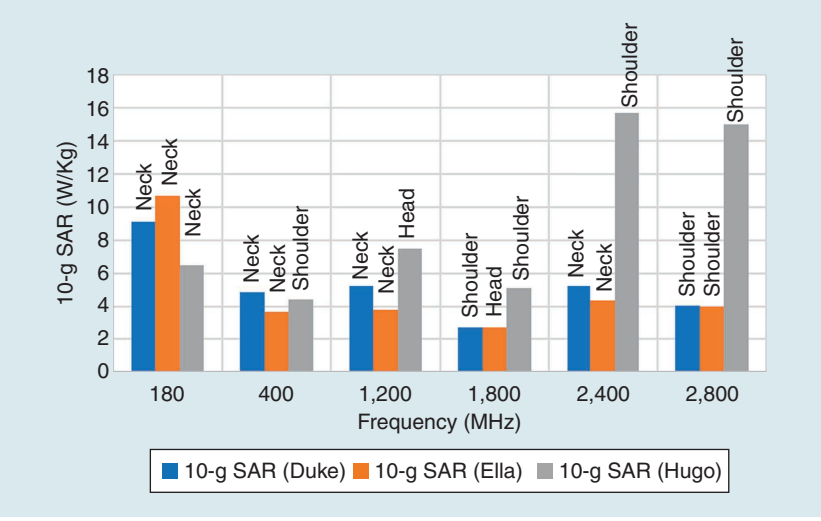

FIGURE 10. The maximum 10-g SAR values and body localization for each model on the three subbands.

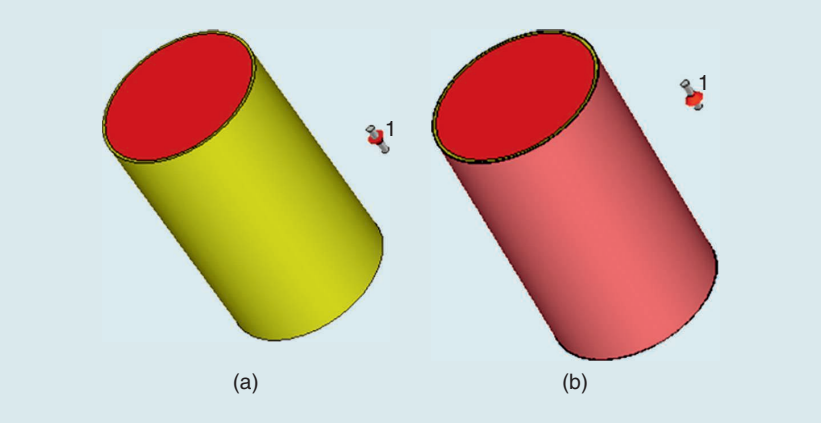

FIGURE 11. The layered cylinders equal to the Hugo torso size, illuminated by the UWB dipole (1,500–2,700 MHz): (a) two layers of muscle and fat and (b) three layers of muscle, fat, and skin.

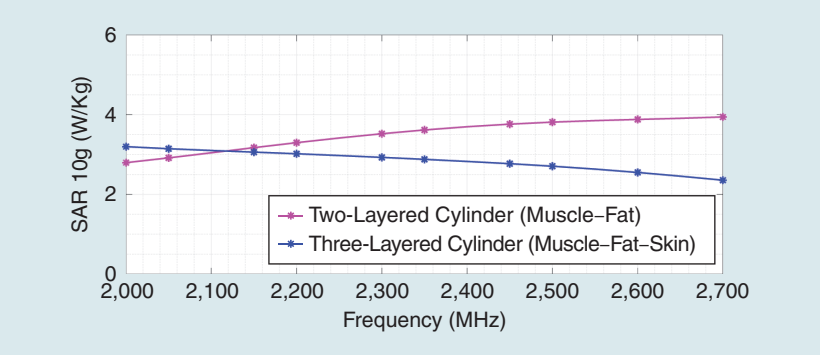

FIGURE 12. The 10-g SAR estimation trend for a peak input power equal to 60 W, evaluated for the two-layer (muscle–fat) and three-layer (muscle–fat–skin) cylinders. It can be noticed that the skin presence drastically reduces the SAR level for the same input power.

assumption is that the cylinders were irradiated by the UWB dipole (1,500–2,700 MHz), placed 13 cm from their surface, to simulate the same realistic scenario represented in Figure 6.

The results in terms of the 10-g SAR are given in Figure 12. The results explain what was observed among the three models in terms of SAR differences at this frequency range. Indeed, due to the high permittivity values, the skin prevents antenna signal propagation, shielding the body and minimizing SAR deposition. Indeed, skin acts as a barrier between the antenna and body, especially at higher frequencies, in which the penetration depth is reduced.

In the cylinder without skin, the antenna impedance matching is maximized; the propagation loss is lower, so higher exposure levels result. Although Hugo is one of the most employed voxel models in the literature, the problem of skin absence must be carefully considered when employing this model for exposure assessment.

CONCLUSIONS

In this work, we proposed a systematic electromagnetic energy absorption assessment for human body models of different sexes and body conformations, when exposed to high-intensity, portable, and broadband signal devices. Starting from our previous works, we have modeled radiative sources as realistic backpack devices, generally used for communication or situational awareness purposes in the military field. Three antennas have been specifically designed to faithfully represent the behavior of such broadband radiative systems (40–2,700 MHz) to cover the entire radio communication band. To obtain detailed and accurate exposure levels results, we adopted three realistic human models representative of shape and gender variability (Hugo, Duke, and Ella).

To the best of our knowledge, this is the first systematic literature study where different voxel phantoms exposed to broadband high-power near-field sources are investigated in terms of electromagnetic exposure. We estimated both the WBA-SAR and local 10-g SAR. Regarding the WBA-SAR, significantly higher exposure levels were observed for the female model, due to reduced body weight compared to the male counterparts.

Due to the peculiar application, i.e., where the radiating systems are placed very close to the body, particular attention was focused on the evaluation of the 10-g SAR, as it is significant for localized tissue heating. It was found that at lower frequencies, the presence of a greater percentage of fat in the female model led to increased energy absorption. In addition, the presence of the skin layer increases reflection at higher frequencies, with a consequent reduction in exposure levels.

The results showed that the WBA-SAR is closely related to total body weight. Conversely, the 10-g SAR varies according to the frequency range and with each voxel model. Only in the case of female exposure were the limits imposed by the ICNIRP exceeded for a radiating power of 60 W. The proposed study can be used as a general methodology to infer the risk levels of other critical and high-exposure test cases by performing accurate numerical studies.

AUTHOR INFORMATION

Eliana Canicattì (eliana.canicatti@phd.unipi.it) is with the Department of Information Engineering, University of Pisa, 56122 Pisa, Italy. She is a Student Member of IEEE.

Danilo Brizi (danilo.brizi@unipi.it) is with the Department of Information Engineering, University of Pisa, 56122 Pisa, Italy. He is a Member of IEEE.

Angelica Masi (angelica.masi@phd.unipi.it) is with the Department of Information Engineering, University of Pisa, 56122 Pisa, Italy. She is a Student Member of IEEE.

Nunzia Fontana (nunzia.fontana@unipi.it) is an associate professor with the Department of Energy, Systems, Territory, and Construction Engineering, University of Pisa, 56122 Pisa, Italy. She is a Senior Member of IEEE.

Agostino Monorchio (agostino.monorchio@unipi.it) is with the Department of Information Engineering, University of Pisa, 56122 Pisa, Italy. He is a Fellow of IEEE.

REFERENCES

[1] "The international EMF project," World Health Organization, Geneva, Switzerland, 1994–1995. [Online]. Available: https://www.who.int/initiatives/the-international-emf-project

[2] International Commission on Non-Ionizing Radiation Protection, "Guidelines for limiting exposure to time-varying electric, magnetic, and electromagnetic fields (up to 300 GHz). International commission on non-ionizing radiation protection," *Health Phys.*, vol. 74, no. 4, pp. 494–522, Apr. 1998.

[3] *IEEE Standard for Safety Levels with Respect to Human Exposure to Radio Frequency Electromagnetic Fields, 3 kHz to 300 GHz*, IEEE Standard C95.1-2005 (Revision of IEEE Std C95.1-1991), Institute of Electrical and Electronics Engineers, New York, NY, USA, Apr. 2006.

[4] F. G. Shellock and J. V. Crues, "Temperature, heart rate, and blood pressure changes associated with clinical MR imaging at 1.5 T," *Radiology*, vol. 163, no. 1, pp. 259–262, Apr. 1987, doi: 10.1148/radiology.163.1.3823445.

[5] R. L. Magin, R. P. Liburdy, and B. Persson, *Biological Effects and Safety Aspects of Nuclear Magnetic Resonance Imaging and Spectroscopy*. New York, NY, USA: New York Academy of Sciences, 1992.

[6] P. Bernardi, M. Cavagnaro, S. Pisa, and E. Piuzzi, "Specific absorption rate and temperature increases in the head of a cellular-phone user," *IEEE Trans. Microw. Theory Techn.*, vol. 48, no. 7, pp. 1118–1126, Jul. 2000, doi: 10.1109/22.848494.

[7] J. B. Ferreira, A. A. Almeida de Salles, and C. E. Fernandez-Rodriguez, "SAR simulations of

EMF exposure due to tablet operation close to the user's body," in *Proc. SBMO/IEEE MTT-S Int. Microw. Optoelectronics Conf. (IMOC)*, Porto de Galinhas, Brazil, Nov. 2015, pp. 1–5, doi: 10.1109/IMOC.2015.7369205.

[8] H. Wang, "Analysis of electromagnetic energy absorption in the human body for mobile terminals," *IEEE Open J. Antennas Propag.*, vol. 1, pp. 113–117, Mar. 2020, doi: 10.1109/OJAP.2020.2982507.

[9] S. Kim, Y. Sharif, and I. Nasim, "Human electromagnetic field exposure in wearable communications: A review," 2019. [Online]. Available: http://arxiv.org/abs/1912.05282

[10] P. Bernardi, M. Cavagnaro, S. Pisa, and E. Piuzzi, "SAR distribution and temperature increase in an anatomical model of the human eye exposed to the field radiated by the user antenna in a wireless LAN," *IEEE Trans. Microw. Theory Techn.*, vol. 46, no. 12, pp. 2074–2082, Dec. 1998, doi: 10.1109/22.739285.

[11] M. S. Morelli, S. Gallucci, B. Siervo, and V. Hartwig, "Numerical analysis of electromagnetic field exposure from 5G mobile communications at 28 GHZ in adults and children users for real-world exposure scenarios," *Int. J. Environ. Res. Public. Health*, vol. 18, no. 3, Feb. 2021, Art. no. 1073, doi: 10.3390/ijerph18031073.

[12] K. H. Kuther, I. H. Ali, and R. K. Ahmed, "Radiation effect of fractal sierpinski square patch antenna," *Int. J. Elect. Comput. Eng.*, vol. 10, no. 5, pp. 5329–5334, Oct. 2020, doi: 10.11591/ijece.v10i5.pp5329-5334.

[13] M. Smondrk, M. Benova, and Z. Psenakova, "Specific absorption rate evaluation in human body model comprising of metallic implant," in *Proc. 19th Int. Conf. Comput. Problems Elect. Eng.*, Banska Stiavnica, Slovakia, 2018, pp. 1–4, doi: 10.1109/CPEE.2018.8507101.

[14] F. Kaburcuk and A. Z. Elsherbeni, "SAR and temperature rise distributions in a human head due to a multi-frequency antenna source," in *Proc. Int. Appl. Comput. Electromagn. Soc. Symp. (ACES)*, Denver, CO, USA, Mar. 2018, pp. 1–2, doi: 10.23919/ROPACES.2018.8364205.

[15] S. il Kwak, D.-U. Sim, J. H. Kwon, and Y. J. Yoon, "Design of PIFA with metamaterials for body-SAR reduction in wearable applications," *IEEE Trans. Electromagn. Compat.*, vol. 59, no. 1, pp. 297–300, Feb. 2017, doi: 10.1109/TEMC.2016.2593493.

[16] A. Shah and P. Patel, "E-textile slot antenna with spurious mode suppression and low SAR for medical wearable applications," *J. Electromagn. Waves Appl.*, vol. 35, no. 16, pp. 2224–2238, Nov. 2021, doi: 10.1080/09205071.2021.1934905.

[17] *IEEE Standard for Military Workplaces--Force Health Protection Regarding Personnel Exposure to Electric, Magnetic, and Electromagnetic Fields, 0 Hz to 300 GHz*, IEEE Standard C95.1-2345-2014, May 2014.

[18] E. Canicatti, E. Giampietri, D. Brizi, N. Fontana, and A. Monorchio, "A numerical exposure assessment of portable self-protection, high-range, and broadband electromagnetic devices," *IEEE Open J. Antennas Propag.*, vol. 2, pp. 555–563, Apr. 2021, doi: 10.1109/OJAP.2021.3072548.

[19] M. A. Bredella, "Sex differences in body composition," in *Sex and Gender Factors Affecting Metabolic Homeostasis, Diabetes and Obesity*, vol. 1043, F. Mauvais-Jarvis, Ed. Cham, Switzerland: Springer International Publishing, 2017, pp. 9–27.

[20] H. Homann, P. Börnert, H. Eggers, K. Nehrke, O. Dössel, and I. Graesslin, "Toward individualized SAR models and in vivo validation: Individualized SAR models," *Magn. Reson. Med.*, vol. 66, no. 6, pp. 1767–1776, Dec. 2011, doi: 10.1002/mrm.22948.

[21] H. Homann et al., "Local SAR management by RF Shimming: A simulation study with multiple human body models," *Magn. Reson. Mater. Phys., Biol. Med.*, vol. 25, no. 3, pp. 193–204, Jun. 2012, doi: 10.1007/s10334-011-0281-8.

[22] A. Hirata, I. Laakso, T. Oizumi, R. Hanatani, K. H. Chan, and J. Wiart, "The relationship between specific absorption rate and temperature elevation in anatomically based human body models for plane wave exposure from 30 MHz to 6 GHz," *Phys. Med. Biol.*, vol. 58, no. 4, pp. 903–921, Jan. 2013, doi: 10.1088/0031-9155/58/4/903.

[23] L. Sandrini, A. Vaccari, C. Malacarne, L. Cristoforetti, and R. Pontalti, "RF dosimetry: A comparison between power absorption of female and male numerical models from 0.1 to 4 GHz," *Phys. Med. Biol.*, vol. 49, no. 22, pp. 5185–5201, Oct. 2004, doi: 10.1088/0031-9155/49/22/012.

[24] P. J. Dimbylow, A. Hirata, and T. Nagaoka, "Intercomparison of whole-body averaged SAR in European and Japanese voxel phantoms," *Phys. Med. Biol.*, vol. 53, no. 20, pp. 5883–5897, Sep. 2008, doi: 10.1088/0031-9155/53/20/022.

[25] P. Dimbylow, "Resonance behaviour of whole-body averaged specific energy absorption rate (SAR) in the female voxel model, NAOMI," *Phys. Med. Biol.*, vol. 50, no. 17, pp. 4053–4063, Aug. 2005, doi: 10.1088/0031-9155/50/17/009.

[26] DiPP GmbH, Apr. 2013, "Anatomical volume data sets," DiPP GmbH. [Online]. Available: http://www.vr-laboratory.com

[27] "Human models," IT'IS Foundation, Zurich, Switzerland. [Online]. Available: https://itis.swiss/virtual-population/virtual-population/overview/

[28] E. Canicatti, E. Giampietri, D. Brizi, N. Fontana, and A. Monorchio, "SAR evaluation from high-intensity and broadband sources for different human body models," in *Proc. IEEE Int. Symp. Antennas Propag. USNC-URSI Radio Sci. Meeting (APS/URSI)*, Singapore, 2021, pp. 359–360, doi: 10.1109/APS/URSI47566.2021.9703715.

[29] N. Fontana, E. Giampietri, E. Canicatti, D. Brizi, and A. Monorchio, "Broadband numerical evaluation of SAR distribution due to high-intensity radiated fields by portable systems," in *Proc. IEEE Int. Symp. Antennas Propag. North Amer. Radio Sci. Meeting*, Montreal, QC, Canada, 2020, pp. 307–308, doi: 10.1109/IEEECONF35879.2020.9329849.

[30] R. Y. Ha, K. Nojima, W. P. Adams, and S. A. Brown, "Analysis of facial skin thickness: Defining the relative thickness index," *Plastic Reconstructive Surgery*, vol. 115, no. 6, pp. 1769–1773, May 2005, doi: 10.1097/01.PRS.0000161682.63535.9B.

[31] "Visible human project," The National Library of Medicine, Bethesda, MD, USA. [Online]. Available: http://www.nlm.nih.gov/research/visible/visible_human.html

[32] A. Christ et al., "The virtual family—Development of surface-based anatomical models of two adults and two children for dosimetric simulations," *Phys. Med. Biol.*, vol. 55, no. 2, pp. N23–N38, Dec. 2010, doi: 10.1088/0031-9155/55/2/N01.

[33] S. Gabriel, R. W. Lau, and C. Gabriel, "The dielectric properties of biological tissues: III. Parametric models for the dielectric spectrum of tissues," *Phys. Med. Biol.*, vol. 41, no. 11, pp. 2271–2293, Nov. 1996, doi: 10.1088/0031-9155/41/11/003.

[34] A. D. Tinniswood, C. M. Furse, and O. P. Gandhi, "Power deposition in the head and neck of an anatomically based human body model for plane wave exposures," *Phys. Med. Biol.*, vol. 43, no. 8, pp. 2361–2378, Aug. 1998, doi: 10.1088/0031-9155/43/8/026.

[35] J. M. Ziriax et al., "Effects of frequency, permittivity, and voxel size on predicted specific absorption rate values in biological tissue during electromagnetic-field exposure," *IEEE Trans. Microw. Theory Techn.*, vol. 48, no. 11, pp. 2050–2058, Nov. 2000, doi: 10.1109/22.884194.

[36] A. Ijjeh, M. Cueille, J.-L. Dubard, and M. Ney, "Modeling finite-radius VHF and HF wire-antennas for numerical dosimetry applications in near-field interaction scenarios," in *Proc. 15th Eur. Conf. Antennas Propag. (EuCAP)*, Dusseldorf, Germany, Mar. 2021, pp. 1–5, doi: 10.23919/EuCAP51087.2021.9411288.

[37] *IEC/IEEE International Standard -- Determining the Peak Spatial-Average Specific Absorption Rate (SAR) in the Human Body from Wireless Communications Devices, 30 MHz to 6 GHz – Part 1: General Requirements for Using the Finite-Difference Time-Domain (FDTD) Method for SAR Calculations*, IEC/IEEE International Standard 62704-1:2017, 2017.

[38] "Assessing the compliance of emissions from HF broadcast transmitters," European Broadcasting Union, Geneva, Switzerland, Tech. Rev. 306, Apr. 2006. [Online]. Available: https://tech.ebu.ch/publications/trev_306-emf_hf

[39] Institute of Electrical and Electronics Engineers, *2013 International Symposium on Electromagnetic Compatibility (EMC Europe 2013)*. Piscataway, NJ, USA: IEEE, 2013.

[40] E. Conil, A. Hadjem, F. Lacroux, M. F. Wong, and J. Wiart, "Variability analysis of SAR from 20 MHz to 2.4 GHz for different adult and child models using finite-difference time-domain," *Phys. Med. Biol.*, vol. 53, no. 6, pp. 1511–1525, Mar. 2008, doi: 10.1088/0031-9155/53/6/001.

[41] Y. Guo, J. Wang, H.-K. Ma, L.-D. Wang, and W.-Y. Yin, "Specific absorption rate (SAR) evaluation of human body model in the presence of radar wave radiation on a warship deck," in *Proc. IEEE Int. Symp. Electromagn. Compat. (EMC)*, Dresden, Germany, 2015, pp. 541–545, doi: 10.1109/ISEMC.2015.7256220.

[42] I. VilasBoas-Ribeiro, G. C. van Rhoon, T. Drizdal, M. Franckena, and M. M. Paulides, "Impact of number of segmented tissues on SAR prediction accuracy in deep pelvic hyperthermia treatment planning," *Cancers*, vol. 12, no. 9, Sep. 2020, Art. no. 2646, doi: 10.3390/cancers12092646.

[43] N. B. Asan et al., "Intra-body microwave communication through adipose tissue," *Healthcare Technol. Lett.*, vol. 4, no. 4, pp. 115–121, May 2017, doi: 10.1049/htl.2016.0104.

[44] M. Sarestoniemi, C. Pomalaza-Raez, C. Kissi, M. Berg, M. Hamalainen, and J. Iinatti, "WBAN channel characteristics between capsule endoscope and receiving directive UWB on-body antennas," *IEEE Access*, vol. 8, pp. 55,953–55,968, Mar. 2020, doi: 10.1109/ACCESS.2020.2982247.

[45] E. M. Staderini, "UWB radars in medicine," *IEEE Aerosp. Electron. Syst. Mag.*, vol. 17, no. 1, pp. 13–18, Jan. 2002, doi: 10.1109/62.978359.

[46] M. Cavagnaro, S. Pisa, and E. Pittella, "Safety aspects of human exposure to ultra wideband radar fields," in *Proc. Int. Symp. Electromagn. Compat. – EMC EUROPE*, Rome, Italy, 2012, pp. 1–5, doi: 10.1109/EMCEurope.2012.6396885.

[47] P. Störchle, W. Müller, M. Sengeis, S. Lackner, S. Holasek, and A. Fürhapter-Rieger, "Measurement of mean subcutaneous fat thickness: Eight standardised ultrasound sites compared to 216 randomly selected sites," *Sci. Rep.*, vol. 8, no. 1, Nov. 2018, Art. no. 16268, doi: 10.1038/s41598-018-34213-0.

[48] Y. Lee and K. Hwang, "Skin thickness of Korean adults," *Surgical Radiologic Anatomy*, vol. 24, nos. 3–4, pp. 183–189, Aug./Sep. 2002, doi: 10.1007/s00276-002-0034-5.